Eur. Phys. J. B **58**, 345–351 (2007)
DOI: 10.1140/epjb/e2007-00232-2

THE EUROPEAN PHYSICAL JOURNAL B

Phase separation dynamics in small-world media

R. Imayama and Y. Shiwa[a]

Statistical Mechanics Laboratory, Kyoto Institute of Technology, Matsugasaki, Sakyo-ku, Kyoto 606-8585, Japan

Received 31 March 2007 / Received in final form 24 July 2007
Published online 8 September 2007 –

Abstract. We present results of a numerical study of phase separation dynamics of a two-dimensional quenched system which has a small-world topology, both with and without the conserved order parameter. We examine how the domain coarsening changes with the density of long-range connections (shortcuts). It is demonstrated that the shortcuts have directly opposite effects, i.e., a speeding up of the coarsening process of reaching a fully uniform state, and a freezing of the system in a disordered metastable state.

PACS. 89.75.Fb Structures and organization in complex systems – 47.54.-r Pattern selection; pattern formation – 64.60.Cn Order-disorder transformations; statistical mechanics of model systems

1 Introduction

When a system is quenched from high temperature to zero temperature, the system develops order from disorder through domain growth and coarsening (phase separation). For systems with homogeneous structures such as pure binary fluids and alloys, it is well established [1] that at late stages of this phase-ordering dynamics, the system is characterized by a single dynamic length scale $\ell(t)$ that grows with time as a power law, $\ell(t) \sim t^{\alpha}$. For inhomogeneous systems our understanding of phase separation kinetics is poorer at a much preliminary level, although such systems abound in nature spanning many disciplines in science from physics and chemistry to biology.

In this connection, a recent surge of interest in complex networks is noteworthy (see reviews [2–5]). The notion of a network can describe any system whose constituent entities (referred to as node or vertex of the network) interact with each other. Each interaction between nodes results in a link (edge) between them. Typical features shared by many complex networks are the small-world property [6] and the scale-free structure [7]. The scale-free structure refers to the absence of a characteristic scale in the distribution of the number of links of a node, giving rise to a large connectivity heterogeneity. The small-world effect refers to a high degree of clustering of nodes as well as the small number of links in shortest paths between nodes.

The small-world (SW) property is usually exhibited by complex systems which have a regular topology modified by an increasing density of random long-range connections [6,8,9]. The question we address in this paper is how such SW network structure controls the phase-ordering processes taking place on the network. Specifically we study the effect of long-range links in the SW network on the phase separation. It turns out that the SW topologies give rise to a nonequilibrium transition between an inhomogeneous phase of coexisting regions with different values of the order parameter (ψ) and a phase with all the system sharing a common value of ψ.

The SW network we consider in this work is constructed as follows [9]. We start with a two-dimensional square lattice. We then add shortcuts between pairs of vertices chosen uniformly at random but we do not remove any bonds from the regular lattice. More than one bond between any two vertices as well as any bond connecting a vertex to itself are prohibited. In particular, we add with probability p one shortcut for each bond on the original lattice, so that an average coordination number z is given by $z = 4(1 + p)$.

On this SW network, evolution of the order parameter ψ_i to be defined at each vertex site i is described by the zero-noise Langevin equation [10]

$$\frac{\partial \psi_i}{\partial t} = -L(\nabla^2)[-r\psi_i + u\psi_i^3 - D\nabla^2\psi_i]. \qquad (1)$$

Here $L(\nabla^2)$ is a constant Γ_0 for a nonconserved order parameter (NCOP, or model A), while $L(\nabla^2) = -M\nabla^2$ for the conserved order parameter (COP, or model B); in the following we set $\Gamma_0 = M = 1$ in appropriate units. The positive constants r, u and D are phenomenological parameters. The diffusive coupling is represented by the Laplacian operator, which is fully characterized by the adjacency matrix a_{ij}, taking the value $a_{ij} = 1$ if the vertices i and j are connected by an edge, whereas $a_{ij} = 0$ otherwise. Namely, for any quantity X_i on the vertex i of the network

$$\nabla^2 X_i = \sum_j (a_{ij} - k_i\delta_{ij})X_j, \qquad (2)$$

[a] e-mail: shiway@kit.ac.jp

where k_i is the degree of the vertex i, $k_i = \sum_j a_{ij}$. Here and hereafter we have set the lattice spacing $\triangle x$ of the square lattice to unity, $\triangle x = 1$. In passing we remark that a matrix $D_{ij} \equiv a_{ij} - k_i\delta_{ij}$ in equation (2) is a diffusion matrix defined on the underlying discrete network and is a conservative operator [11].

In the next section, we describe different pattern planforms expected from the mean-field treatment of equation (1). Results of detailed simulations are presented in Section 3. The final section contains a summary and discussion of the results.

2 Possible morphologies

In the mean-field approximation to the evolution equation (1), random long-range links are replaced with their expected number, i.e., each site is linked to all others via a shortcut of strength $4p/N$, where N is the total number of vertices in the network. Hence

$$\nabla^2\psi_i = (\nabla^2)^{nn}\psi_i + 4p(\bar{\psi} - \psi_i), \tag{3}$$

where $(\nabla^2)^{nn}$ is the Laplacian on the original regular lattice, and $\bar{\psi} = (1/N)\sum_j \psi_j$. With $\psi \equiv \psi_i$ and $\nabla^2 \equiv (\nabla^2)^{nn}$ for simplicity, equation (1) reduces to

$$\frac{\partial\psi}{\partial t} = (r - 4pD)\psi - u\psi^3 + D\nabla^2\psi + 4pD\bar{\psi} \tag{4}$$

for NCOP, and

$$\begin{aligned}\frac{\partial\psi}{\partial t} = {} & \nabla^2(-\tilde{r}\psi + u\psi^3 - D\nabla^2\psi) - B(\psi - \bar{\psi}) \\ & -C(\psi^3 - \overline{\psi^3})\end{aligned} \tag{5}$$

for COP with

$$\tilde{r} \equiv r - 8pD, \quad B \equiv 4p(4pD - r), \quad C \equiv 4pu, \tag{6}$$

and $\overline{\psi^3} \equiv (1/N)\sum_j \psi^3$. Notice in equation (5) that when shortcuts are present, one obtains the nongradient cubic coupling ($\propto C$). In contrast, in the NCOP case we have the gradient dynamics (4) with the Lyapunov (effective free energy) functional

$$\begin{aligned}F = {} & \frac{1}{2}\int d\boldsymbol{r}\Big\{(4pD - r)\psi^2(\boldsymbol{r}) + D\big(\nabla\psi(\boldsymbol{r})\big)^2 + \frac{u}{2}\psi^4(\boldsymbol{r}) \\ & -\frac{4pD}{V}\int d\boldsymbol{r}'\psi(\boldsymbol{r}')\psi(\boldsymbol{r})\Big\},\end{aligned} \tag{7}$$

where V is the volume of the system.

It is then easy to show that in systems with NCOP a uniform state (in which $\psi = \psi^* \equiv \sqrt{r/u}$ or $\psi = -\psi^*$) is always selected when $p \neq 0$. In the case $p = 0$, one recovers the usual situation where, depending on the degree of off-criticality, either the uniform phase or the inhomogeneous phase with two degenerate states $\psi = \pm\psi^*$ coexisting is realized.

In the COP case, the linear stability analysis of equation (5) yields the following consequences:

- for $r > r_c \equiv 4pD + 3u\bar{\psi}^2$, one obtains the inhomogeneous phase in which two homogeneous states $\psi = \pm\psi_0$ coexist, where $\psi_0 \equiv \sqrt{(r - 4pD)/u}$. We remark that the morphology in this case depends on $\bar{\psi}$. For the critical quench ($\bar{\psi} = 0$), there is symmetry between the two competing states resulting in convoluted percolating patterns. When the system moves off-critical, this symmetry is broken and droplet pattern may appear;
- for $r \leq r_c$, the uniform state with $\psi = \bar{\psi}$ is stable.

3 Numerical results

We have performed simulations based on equation (1). In order to allow efficient exploration of the long-time regime of phase-ordering kinetics, we follow the spirit of the cell-dynamical-system (CDS) method [12]. A two-dimensional space is divided into 256×256 square cells with periodic boundary conditions. For equation (1) we solve the following CDS model of the order parameter $\psi(n,t)$ associated with a lattice site labeled by n at time t:

$$\psi(n,t+1) = \begin{cases}\mathcal{F}\big\{\psi(n,t)\big\} & \text{for NCOP} \\ \psi(n,t) - \nabla^2\big[\mathcal{F}\{\psi(n,t)\} - \psi(n,t)\big] & \\ & \text{for COP}\end{cases} \tag{8}$$

with

$$\mathcal{F}\{\psi(n,t)\} \equiv A\tanh\psi(n,t) + D\nabla^2\psi(n,t). \tag{9}$$

The Laplacian is evaluated as given in equation (2). In the following we present first our numerical results of NCOP and then the results of COP.

3.1 NCOP

For the NCOP, we have fixed the parameters as $A = 1.2$ and $D = 0.1$ with varying values of the connection probability p. For a given p, we have numerically integrated equation (8) with the initial configurations of $\psi(n,t)$ at each site n randomly chosen to have the values $\delta\psi \pm a$, where $a = 0.01$ with different choices of $\delta\psi$. The a represents fluctuations in the initial state and $\delta\psi$ is a measure of how far off-critical the system is placed at $t = 0$ (hence the particular case $\delta\psi = 0$ corresponds to a critical quench). We measured the time-dependent magnitude of the mean order parameter $\bar{\psi}(t)$. The average magnitude $\langle|\bar{\psi}(t)|\rangle$ was then calculated as an average over five realizations of different networks at each value of p.

We have found that the behavior of time evolution of $\langle|\bar{\psi}(t)|\rangle$ changes substantially with $\delta\psi$. Namely, if $\delta\psi/a \gtrsim 0.2$, the system equilibrates over a rather short time scale to a homogeneous state (Fig. 1). On the other hand, in the range $\delta\psi/a < 0.2$, $\langle|\bar{\psi}(t)|\rangle$ has a power-law growth

$$\langle|\bar{\psi}(t)|\rangle \sim t^{\alpha} \tag{10}$$

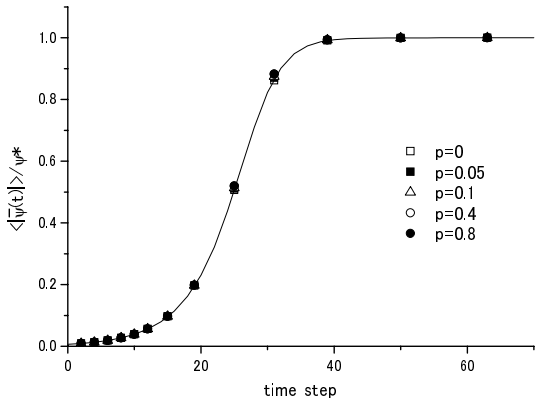

Fig. 1. Temporal evolution of the normalized $\langle|\bar{\psi}(t)|\rangle$ for the off-critical quench with $\delta\psi = 0.005$. The ψ^* is the equilibrium value of ψ. The results for five distinct connection probabilities are shown. The solid curve is a mean-field theoretical result: $\langle|\bar{\psi}(t)|\rangle/\psi^* = \left\{1 - \left[1 - (\psi^*/\delta\psi)^2\right]\exp(-2B{\psi^*}^2 t)\right\}^{-1/2}$, which is obtained from equation (4). The B is the fitting parameter to account for the different units of space and time of CDS dynamics.

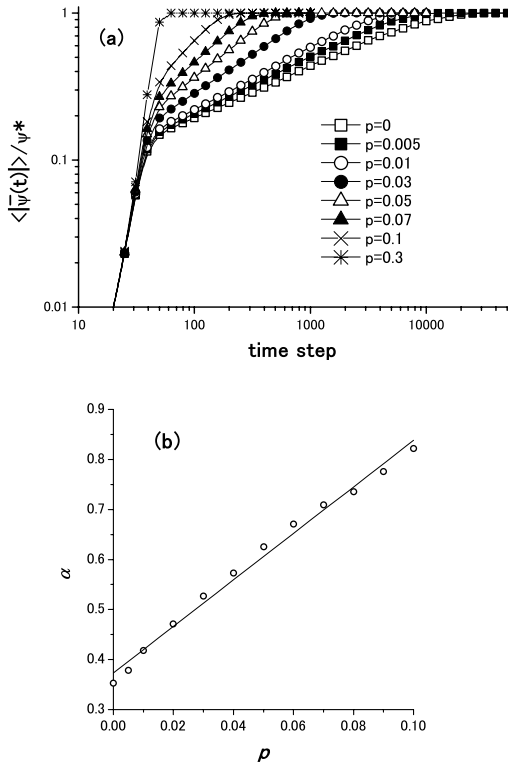

Fig. 2. (a) Temporal evolution of $\langle|\bar{\psi}(t)|\rangle/\psi^*$ for $\delta\psi = 0.0002$ and various values of p. (b) Growth exponent α as a function of p. The solid line is best fit to the data.

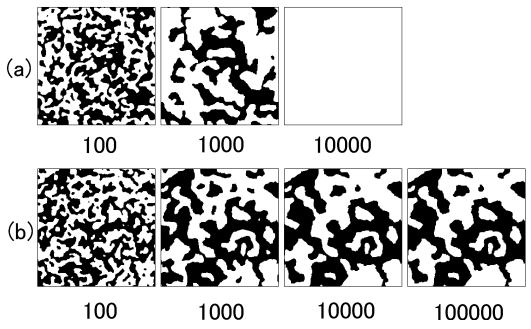

Fig. 3. Pattern evolution in the critical quench of NCOP for $p = 0.05$, leading to either (a) a homogeneous state or (b) a frozen state. The white region represents positive values of the order parameter ψ and the black one negative ψ. The numbers denote the necessary time steps from the same initial condition.

before the system reaches the final equilibrium homogeneous state. To illustrate this, we give in Figure 2a a plot of $\langle|\bar{\psi}(t)|\rangle$ against t for varying connection probabilities p at $\delta\psi/a = 0.02$. Notice that when the value of p is increased, the time interval over which the power-law growth is observed shrinks with the concurrent increase of the growth exponent α. Figure 2b demonstrates that the growth exponent varies as $\alpha \propto p$. These features should be compared with the radically different behavior given in Figure 1, where numerical data for different p's superpose well over the entire time domain.

An important remark is in place here before proceeding to results for the COP case. In our simulations of *critical quenches* for small $p \ll 1$, we have encountered several runs in which metastable states persist and the system gets stuck in these states without reaching the equilibrium homogeneous state. A typical snapshot of this frozen state is shown in Figure 3b as compared with the ordinary nonfreezing case (Fig. 3a).

One might argue that such frozen states are possibly due to a finite-size effect of the system, and expect that the probability for such states to exist approaches zero in the thermodynamic limit. To test this, we measured the probability $P_F(L)$ to reach a frozen configuration on $L \times L$ SW lattices in the case $p = 0.05$ as a function of L for $L \leq 500$. Our result shown in Figure 4 apparently fails to meet the expectation, and suggests that $P_F(L)$ approaches a nonzero value as $L \to \infty$. Nonetheless, the possibility that the observed frozen configuration could be a long-lived transient is certainly worth investigating further.

In this connection we point out that in the kinetics of ordering in two-dimensional zero-temperature Ising model of order-disorder transitions, a nonzero probability of reaching frozen metastable states has been reported [13]. It should be stressed, however, that the frozen configuration found in the cited studies is domains of a slablike shape, in contrast to the interconnected structure (Fig. 3b) observed in our simulations. This is because the curvature provides a driving force for the domain growth in the Ising dynamics, so that a very small curvature of the strip geometry is the cause leading to formation of the pinned metastable state. The physical situation in our SW media is quite different. The disordered environment created by random long-range connections tends to distort the otherwise circular domains (that are formed in the late stage of phase separation) in such a way to

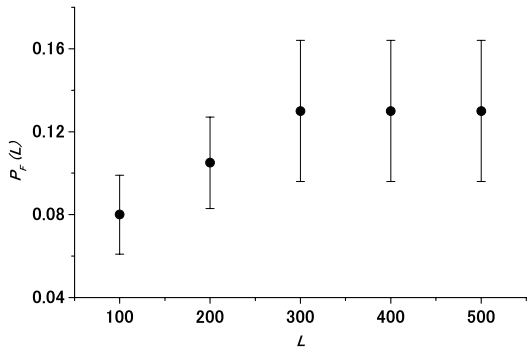

Fig. 4. Probability $P_F(L)$ that an $L \times L$ SW system for $p = 0.05$ eventually reaches a frozen state in critical quenches. Each data point (with error bars) is based on the average over 200 realizations of different networks for $L = 100, 200$ and 100 realizations for $L \geq 300$.

occupy as many favorable pinning sites as possible. It thus gives rise to a complex energy landscape which consists of many different configurations that are locally stable. Such a structure is in fact found in our frozen configurations, as demonstrated in Figure 5.

The metastable configurations which lead to the arrested state should be depinned by random noise. This is demonstrated in Figure 6. It is seen that adding random noise can bring the system out of these metastable states to resume the domain growth.

3.2 COP

We have performed simulations using the COP equation (8) on a 256×256 SW lattice with periodic boundary conditions. Throughout this section, the parameter values we use are $A = 1.016$, $D = 0.008$, and the initial configuration is always with order parameter values of amplitudes $\psi = \delta\psi \pm 0.1$ uniformly and randomly distributed; in critical quenches $\delta\psi = 0$, while for off-critical quenches we use $\delta\psi = 0.08$ (other runs using different values of $\delta\psi$ were done with consistent results). Figures 7 and 8 show a typical pattern evolution for the critical and the off-critical case, respectively. In accord with the mean-field theory, the asymptotic domain morphology changes from an inhomogeneous state with two-phase coexistence to a homogeneous state by the increase of shortcut density. What the mean-field theory fails to predict, however, is that in the simulations the system always becomes pinned at metastable states in the SW regime (Figs. 7c and 8c). We thus looked at the frozen dynamic behavior, and found that the formation of regions trapped in the metastable states can be traced to the nodes with long-range connections. This feature is already described in the previous section, and we shall not repeat the similar analysis here.

In order to make a quantitative analysis of the domain growth, we measured the circularly averaged structure function $S(k,t)$ defined by

$$S(k,t) = \langle \tilde{\phi}(\boldsymbol{k},t)\tilde{\phi}^*(\boldsymbol{k},t)\rangle. \tag{11}$$

Here $\tilde{\phi}(\boldsymbol{k},t)$ is the Fourier transform of the order-parameter fluctuation field ϕ: $\phi(\boldsymbol{r},t) = \psi(\boldsymbol{r},t) - \langle\psi(\boldsymbol{r},t)\rangle$ with the angular brackets denoting statistical averaging. The angular brackets in the above (11) refer to an average over the orientation of the wave vector $\boldsymbol{k}$ as well as an ensemble average; each run is repeated with five different realizations of the network topology to average over. To remove any effect due to the finiteness of the ratio of the thickness of domain walls to the domain size, we calculated $S(k,t)$ after the data were hardened using the transformation $\psi(\boldsymbol{r}) \to \mathrm{sgn}[\psi(\boldsymbol{r})]$. As a measure of the length scale in the description of phase separation kinetics, we use

$$\ell(t) \equiv 2\pi\langle k\rangle^{-1}(t), \tag{12}$$

where $\langle k\rangle(t)$ is the first moment of $S(k,t)$.

A plot of the characteristic length scale $\ell(t)$ thus obtained against t is given in Figure 9 for the critical quench. Note that, in the time regime where the power-law behavior is observed, the growth dynamics speed up by adding shortcuts. For $p > 0.1$, phase separation eventually comes to an end at late times. In this case we also note that by adding more shortcuts, $\ell(t)$ comes to arrest at smaller values of time steps.

We have carried out the same analysis for simulations of off-critical quenches. Apart from the fact that the minority phase forms compact structures, the qualitative features of domain coarsening were essentially the same as those for critical quenches.

One of the most important results that have been obtained for the dynamics of phase separation in systems with a regular topology (i.e., systems without any long-range connection) is the following. Namely, due to the existence of only one length scale, denoted here by $\ell(t)$ again, the late time evolution of the structure function can be described in terms of scaling with $\ell(t)$:

$$S(k,t) = \ell(t)^2\mathcal{T}\big(k\ell(t)\big) \tag{13}$$

in two dimensions, where $\mathcal{T}(x)$ is the time-independent function called scaling function [1]. We thus ask whether the dynamic scaling (13) is satisfied when one introduces the long-range connections into the regular topology. In order to answer this question, we plot in Figure 10 the scaled structure function $S(k,t)/\ell^2(t)$ as a function of the scaled wavenumber $k\ell(t)$ for critical quenches at $p = 0$ and $p = 0.01$ for which the asymptotic behavior of $\ell(t)$ is observed to obey the power law. Within the accuracy of the data [1], the data points for different times lie on a smooth

[1] The peak position of $S(k,t)$ at late stages of coarsening moves toward a small-k value as p increases. Since $S(k,t)$ does not have the self-averaging property for small-k values, we could not get a reliable shape of $S(k,t)$ near $k = 0$ in our simulations. To improve statistics in this wavenumber region, substantially larger systems need to be studied, which is beyond our scope here. Incidentally, in the NCOP case for which $S(k,t)$ is always peaked at $k = 0$, the poor statistics at small k region is even more appreciable at nonzero p. We therefore monitored the quantity in equation (10) rather than the standard $\ell(t)$.

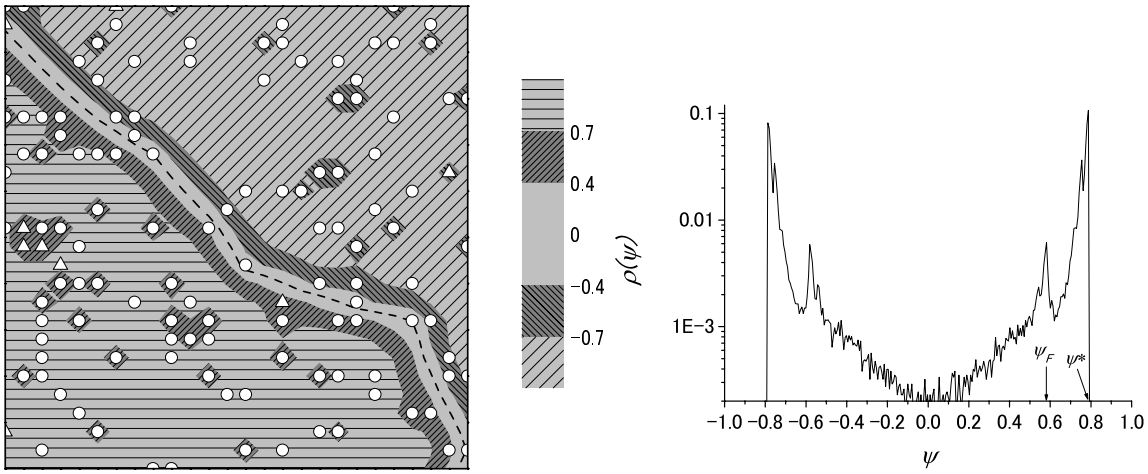

Fig. 5. Left column: grey-scale image of the order parameter field ψ in the frozen asymptotic configuration. The grey levels used for the values of ψ are displayed on the right. The dashed curve represents the domain interface ($\psi = 0$). A 25×25 portion of the 256×256 lattice result for $p = 0.05$ at $t = 10^5$ is exhibited. The circle represents the node which is connected to an other node by a long-range connection (shortcut), while the triangle represents the node connected to two other nodes by shortcuts. Notice that most of the bulk region has reached a configuration in which $\psi \simeq \pm\psi^*$, ψ^* being the equilibrium value of ψ (cf. right column). At positions where nodes having long-range connections are located, the ψ remains pinned at some constant value, $\psi \simeq \pm\psi_F$. Right column: the normalized one-point distribution function $\rho(\psi) \equiv V^{-1} \int d\boldsymbol{r} \delta(\psi - \psi(\boldsymbol{r}))$ in this frozen state. In either positive or negative ψ region, two largest peaks correspond to the equilibrated state ($\psi \simeq \pm\psi^*$) in the bulk, and the third peak (at $\psi = \pm\psi_F$) is caused by the above mentioned arrest at circled or triangled nodes.

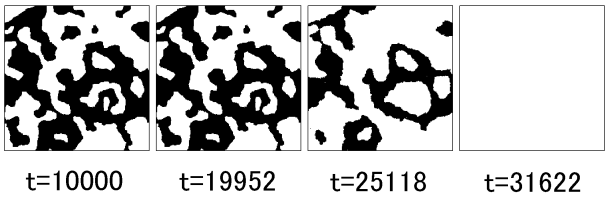

Fig. 6. Depinning of the frozen pattern by noise. At the time step $t = 19952$ at which the frozen configuration depicted in Figure 3b was obtained, we turned on the noise; the noises of amplitude in the range $[-0.12, 0, 12]$ were uniformly and randomly distributed. After 5166 iterations we turned off the noise. The final state that is reached in this experiment is the homogeneous state with $\psi = \psi^*$ (cf. Fig. 5).

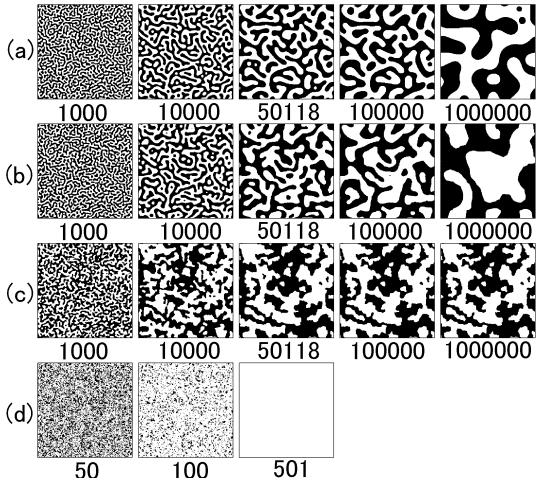

Fig. 7. Pattern evolution in the critical quench: (a) $p = 0$, (b) $p = 0.01$, (c) $p = 0.1$, and (d) $p = 0.9$. The numbers denote necessary time steps from the same initial condition. In (a)–(c) the white regions represent positive values of the order parameter ψ and the black ones negative ψ. In (d) the white regions correspond to $|\psi| \leq 0.01$, while the black ones to $|\psi| > 0.01$. For large values of p as in (d), the homogeneous state $\psi = 0$ is quickly achieved in a short time.

master curve and the scaling ansatz (13) seems to be well satisfied. (We remark, however, that very long times cannot be fitted to the same master curve[2].) Nonetheless, on the basis of these plots, it is unlikely that the scaling function remains universal for different connection probabilities.

4 Summary and discussion

We have studied the dynamics of phase separation in systems with the small-world topology through simulations of the Langevin equations. Systems with both conserved and nonconserved order parameters are considered.

We found that there exists a strong correlation between the growth kinetics and the probability p of adding random long-range shortcuts on each local link of the original regular lattice. For conserved systems, the ordering dynamics is facilitated by the long-range connections in the so-called small-world limit, $p \ll 1$, in which the high clustering[3] among nodes are still present like regular lattices.

[2] A similar behavior of the scaled structure function has been noted in model-B simulations on a regular lattice [14].

[3] For the SW square lattice, the standard clustering coefficient (denoted by C) is identically zero [15]. However, this is

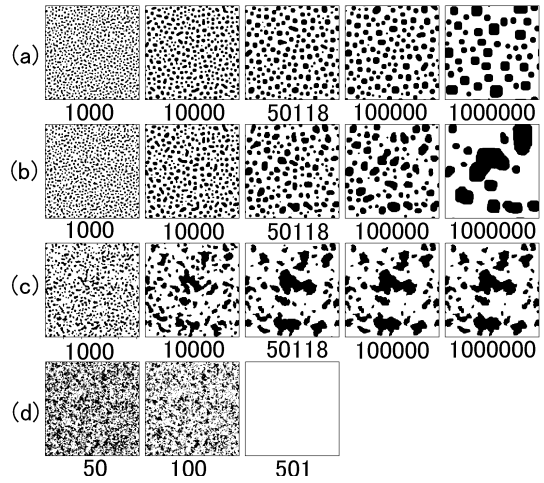

Fig. 8. Pattern evolution in the off-critical quench: (a) $p = 0$, (b) $p = 0.01$, (c) $p = 0.1$, and (d) $p = 0.9$. The numbers denote necessary time steps from the same initial condition. In (a)–(c) the white regions represent positive values of the order parameter ψ and the black ones negative ψ. In (d) the white regions correspond to $\psi \geq 0.99 \times \delta\psi$, while the black ones to $\psi < 0.99 \times \delta\psi$. In qualitative agreement with the mean-field prediction, for large values of p as in (d), the homogeneous state $\psi = \delta\psi$ is quickly achieved in a short time.

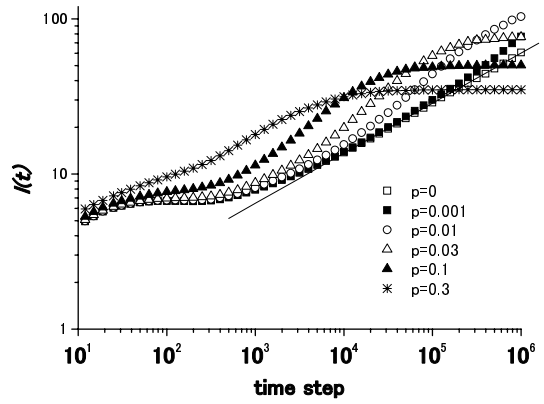

Fig. 9. Time dependence of the characteristic length $\ell(t)$ in critical quenches at various shortcut probabilities p. The solid line is best fit to the $p = 0$ data at late times, which has a slope=0.32 showing the standard $t^{1/3}$ growth [1]. Apparent saturation in the case of $p = 0.01$ is due to finite-size effects as $\ell(t) \sim L/2$ at $t \sim 10^5$, L being the linear size of the system.

Here a power-law growth of the domain size is observed. However, at larger values of p as long as the small-world effects are present, the coarsening gets trapped in partially ordered metastable states. As p is raised further into the random-lattice regime where short and long range connections are equally likely, the system achieves the uniform state in a very short time. These results are insensitive to the initial conditions, i.e., independent of whether the initial state is completely random and symmetric or corresponds to an off-critical quench with asymmetric random initial conditions.

For nonconserved systems, the uniform state is always the equilibrium state for any $p \neq 0$. The ordering dynamics is different, however, depending on the degree of off-criticality of initial conditions. For weakly off-critical quenches (including the symmetric initial conditions), the convergence towards the completely uniform state is of power-law, and the growth exponent increases with p. On the other hand, strong off-criticalities lead to immediate equilibration and the time to achieve this is independent of p. In the case of critical quench, not all realizations of dynamics end up in the uniform state and freezing to a metastable state is found. Our simulations suggest a nonzero value of the probability to enter the metastable state in the limit as $N \to \infty$. We stress that the frozen ordering kinetics cannot be qualitatively accounted for by the mean field theory as given in this paper[4]. As with other disordered systems, devising a formalism able to describe the formation of metastable states remains a theoretical challenge yet to be done.

In connection with the pinning of phase separation processes presented in the present paper, we mention several studies that have observed the similar behavior in other ordering processes on SW lattices. The zero-temperature Glauber dynamics for Ising spins placed on SW networks has been investigated in [19]. The physical arguments are given that frozen metastable states are induced by shortcuts whenever domains attain a characteristic size which scales with some power of $1/p$ as p^{-n} [5]. It is also claimed that this is confirmed by numerical simulations. These results are at variance with our findings. For coarsening systems without disordered topology, it is generally accepted that the Ising model with Glauber dynamics and the model A belong to the same universality class. Consequently, further work needs to be done to resolve this issue, perhaps by numerically studying a much larger system.

Phenomenologically related to the coarsening processes of Ising model is the consensus formation of the voter model [20]. The voter model considers a system with N nodes which represent N voters that have two opinions denoted by $+1$ and -1. Opinion formation of the nodes evolves according to the following updating rule. At each time step, one node is chosen randomly, and is given the opinion value of one of its neighbors that is also chosen at random. The final opinion outcome can then be either a consensus of $+1$ or that of -1. The numerical study [21] of the voter model on SW networks found that the full

due to the misleading artifact of the coefficient C and in fact the square lattice has a generic nonzero clustering characteristic [16,17].

[4] Nontrivial behaviors on complex networks for which the mean field description is inappropriate have previously been found in [18]

[5] In reference [19] the exponent n is determined to be $n = 2/3$. For our COP systems, by contrast, we find from Figure 9 that the domain size $\ell(\infty)$ at which growth stops scales as $\ell(\infty) \sim p^{-1/3}$. As such, both results differ from the characteristic lengthscale ξ_{sc} for shortest paths (the mean separation between shortcut-ends), which scales as $\xi_{sc} \sim p^{-1/2}$ in two-dimensional SW [9].

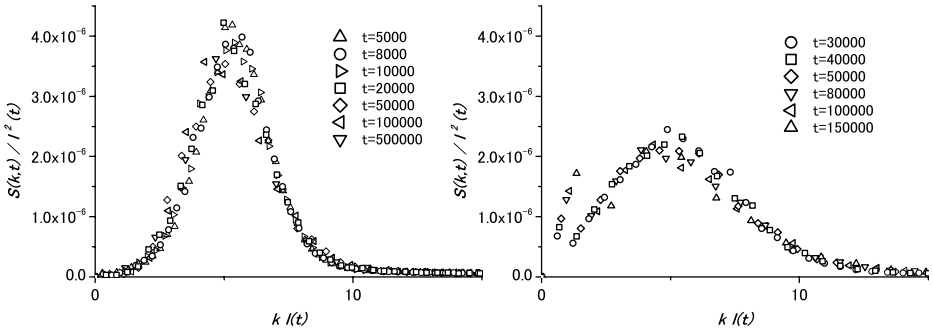

Fig. 10. Scaled structure function $S(k,t)$ with $\ell(t)$ given by equation (12) as the scaling length for critical quenches for $p = 0$ (left) and $p = 0.01$ (right).

consensus is reached provided N is finite. Furthermore, such a complete order is reached in a shorter time than on regular lattices. However, in the thermodynamic limit ($N \to \infty$), the system does not display the complete order.

We should note here that the ordering dynamics in the voter model differs from the Glauber Ising model; in the latter, the evolution is driven by surface tension of domains, whereas in the former model the evolution is based on each voter freely adopting a new state in response to the opinions in his/her connected neighbors. Therefore, a version of voter model put forward by Krapivsky and Redner [22] is more relevant to our work here. The model obeys a local majority updating rule, and the opinion state evolves as follows. At each time step, one node is chosen randomly from the underlying network. The chosen node and its connected neighbors are considered as a group, and all the nodes in the group adopt the state of the local majority. Numerical treatment of this model has been presented in [23]. It is found that the time for reaching full consensus is significantly shortened by the addition of shortcuts. This result is consistent with our results given in Section 3.1, although it is not clear whether the local majority model displays the complete order even in the thermodynamic limit.

To understand the role of underlying heterogeneity in phase separation dynamics, we have confined ourselves to the small-world effects. In real network structures, however, there is another generic feature that is missing from the present analysis. These networks have a highly inhomogeneous structure reflected in their fat-tailed degree distribution $P(k)$ which follows a power law $P(k) \sim k^{-\gamma}$, thus being designated as scale-free networks. Therefore it would be interesting to study how the coarsening dynamics changes in that case, and we plan to present such analysis elsewhere.

References

1. For a review, see A.J. Bray, Adv. Phys. **43**, 357 (1994)
2. R. Albert, A.-I. Barabási, Rev. Mod. Phys. **74**, 47 (2002)
3. S.N. Dorogovtsev, J.F.F. Mendes, Adv. Phys. **51**, 1079 (2002); *Evolution of Networks* (Onford Univ. Press, Oxford, 2003)
4. M.E.J. Newman, SIAM Rev. **45**, 167 (2003)
5. S. Boccaletti, V. Latora, Y. Moreno, M. Chavez, D.-U. Hwang, Phys. Rep. **424**, 175 (2006)
6. D.J. Watts, S.H. Strogatz, Nature (London) **393**, 440 (1998)
7. A.-I. Barabási, R. Albert, Science **286**, 509 (1999)
8. D.J. Watts, *Small Worlds: The Dynamics of Networks Between Order and Randomness* (Princeton Univ. Press, Princeton, 1999)
9. M.E.J. Newman, D.J. Watts, Phys. Rev. E **60**, 7332 (1999)
10. P.C. Hohenberg, B.I. Halperin, Rev. Mod. Phys. **49**, 435 (1977)
11. I. Simonsen, K.A. Eriksen, S. Maslov, K. Sneppen, Physica A **336**, 163 (2004)
12. Y. Oono, S. Puri, Phys. Rev. Lett. **58**, 836 (1987); for more recent references, see A. Shinozaki, Y. Oono, Phys. Rev. E **48**, 2622 (1993)
13. P.S. Sahni, G. Dee, J.D. Gunton, M. Phani, J.L. Lebowitz, M. Kalos, Phys. Rev. B **24**, 410 (1981); V. Spirin, P.L. Krapivsky, S. Redner, Phys. Rev. E **63**, 036118 (2001); see also M.K. Phani, J.L. Lebowitz, M.H. Kalos, O. Penrose, Phys. Rev. Lett. **45**, 366 (1980)
14. S. Puri, Y. Oono, Phys. Rev. A **38**, 1542 (1988)
15. M.E.J. Newman, Computer Phys. Comm. **147**, 40 (2002)
16. G. Caldarelli, R. Pastor-Satorras, A. Vespignani, Eur. Phys. J. B **38**, 183 (2004)
17. R. Imayama, Y. Shiwa (unpublished)
18. C. Castellano, R. Pastor-Satorras, Phys. Rev. Lett. **96**, 038701 (2006); J. Stat. Mech. **5**, P05001 (2006)
19. D. Boyer, O. Miramontes, Phys. Rev. E **67**, 035102(R) (2003)
20. For a recent review, see, e.g., M. San Miguel, V.M. Eguiluz, R. Toral, K. Klemm, Comp. Sci. Eng. **7**, 67 (2005)
21. C. Castellano, D. Vilone, A. Vespignani, Europhys. Lett. **63**, 153 (2003)
22. P.L. Krapivsky, S. Redner, Phys. Rev. Lett. **90**, 238701 (2003)
23. P. Li, D. Zheng, P.M. Hui, Phys. Rev. E **73**, 056128 (2006)